Triplet superconductivity in a model of $Li_{0.9}Mo_6O_{17}$

Natalia Lera[1,2] and J. V. Alvarez[2,3]
[1]*CIC nanoGUNE, 20018 Donostia-San Sebastián, Spain*
[2]*Departamento de Física de la Materia Condensada, Universidad Autónoma de Madrid, 28049 Madrid, Spain*
[3]*Condensed Matter Physics Center (IFIMAC) and Instituto Nicolás Cabrera, Universidad Autónoma de Madrid, 28049 Madrid, Spain*
(Received 5 August 2015; revised manuscript received 7 October 2015; published 19 November 2015)

Superconductivity in the quasi-one-dimensional material $Li_{0.9}Mo_6O_{17}$ is analyzed based on a multiorbital extended Hubbard model. We found strong charge fluctuations at two different momenta $\mathbf{Q_1}$ and $\mathbf{Q_2}$ giving rise to two different charge-ordered phases. Evaluating the superconducting vertex, we found superconductivity near strong charge fluctuations at $\mathbf{Q_1}$. The order parameter has p-wave symmetry with nodes on the Fermi surface. The metallic state displays a characteristic charge collective mode $\mathbf{Q_1}$ due to nesting and, for on-site Hubbard repulsion sufficiently large, a charge critical mode $\mathbf{Q_2}$ driven by Coulomb repulsion, which softens at the proximity to the transition. The results are quite robust for different coupling parametrizations. A phase diagram discussing the relevance of the model to the physics of the material is proposed.

DOI: 10.1103/PhysRevB.92.174523 PACS number(s): 71.10.Hf, 71.10.Fd, 74.40.Kb, 74.70.−b

I. INTRODUCTION

Low-temperature physics of correlated materials is often characterized by the competition between ordered phases and unconventional superconductivity. Typically, a static mean-field description, implying negligible fluctuations beyond the limits of the ordered phase, is not valid in these systems. Nearly all dynamical probes show strong order parameter fluctuations, not only in the neighboring superconducting phases, which suggests a natural mechanism of pairing, but also in the strange metal, present at higher temperatures. Lithium purple bronze (LiPB) adds the ingredient of quasi-one-dimensionality to the problem and suggests the possibility that charge and spin fluctuations alone, without the existence of real order, might be responsible for superconductivity and anomalies of the normal phase.

The metallic phase of LiPB, with chemical formula $Li_{0.9}Mo_6O_{17}$, has been characterized as a robust quasi-one-dimensional material in a series of angle-resolved photoemission spectroscopy (ARPES) experiments ranging through different temperature regimes, sample growth techniques, photon energies, and data analysis procedures [1–9]. Scanning tunneling microscope (STM) spectroscopy shows [10,11] Luttinger liquid (LL) single-particle density of states and thermal and electric transport measurements are in complete disagreement with the Widemann-Franz law [12]. When temperature is decreased, an upturn of the resistivity occurs at $T_m \sim 20$ K [12–15] and the material becomes superconducting at lower temperatures around $T_c \sim 1$ K [14,16].

Unlike other low-dimensional bronzes, the resistivity upturn of LiPB [17] is not associated with a lattice distortion (see Table 1 in Ref. [18]). Neither thermal expansion [19] nor neutron-scattering experiments [20] have identified a phase transition at T_m suggesting the idea of a soft crossover of electronic nature. No gap has been clearly observed in the spectroscopies but optical conductivity measurements [15] suggest the presence of a weak pseudogap. Recently, thermopower [21] and NMR [22] experiments have confirmed different aspects of the quasi-one-dimensionality of this material but the nature of the upturn remains a mystery.

The most recent study of superconducting properties [16] confirms quantitatively that the large anisotropies observed in the upper critical field agree with those expected from the electrical resistivity in the metallic phase. The coherence lengths perpendicular to the chains are larger than interchain distances and H_{c2} increases monotonically with decreasing temperature to values five times larger than the estimated paramagnetic pair-breaking field. Neither spin-orbit scattering nor strong-coupling superconductivity seem to explain this behavior, suggesting the possibility of spin-triplet superconductivity. The specific heat jump ratio is $\frac{\Delta C}{\gamma T_c} = 2.07$ [16]. From a strict BCS theory, this value is closer to the nodeless order parameter $\delta C/\gamma T_c = 1.43$ than to nodal ones, which should give smaller values. A quantitative comparison with experiments [23] shows that superconductivity can be destroyed through orbital effects at fields higher than the Clogston paramagnetic limit *provided* that the superconducting pairs are in the triplet state.

In past years there has been a very important theoretical effort [24–27] to reduce the complexity of the unit cell to microscopic Hamiltonians reproducing different aspects of this phenomenology. In this article, we present a microscopic theory for the unconventional superconducting properties observed in $Li_{0.9}Mo_6O_{17}$. Based on a minimal extended Hubbard model introduced in Refs. [24,25], we show that $Li_{0.9}Mo_6O_{17}$ superconducts in the triplet channel when charge and spin fluctuations are enhanced, which may be also related to the upturn in resistivity at T_m [27]. Using the random-phase approximation (RPA), we identify the charge-density wave (CDW) pattern characterized by two ordering wave vectors, $\mathbf{Q_1}$ and $\mathbf{Q_2}$. In the proximity of those phases we evaluate and analyze the superconducting vertex, finding dominant p-wave triplet superconductivity with nodes on the Fermi surface. Within our methodology we find results compatible with the one presented in a very recent preprint [28].

II. MICROSCOPIC MODEL

The electronic structure close to the E_F and the quasi-one-dimensionality of the system derives from two parallel zigzag Mo-O chains per unit cell [29] (Fig. 1). Tight-binding [30] and density-functional theory (DFT) [31] band-structure calculations agree that the Mo-O orbitals of the chain give rise to four bands and two of them cross the Fermi level. ARPES

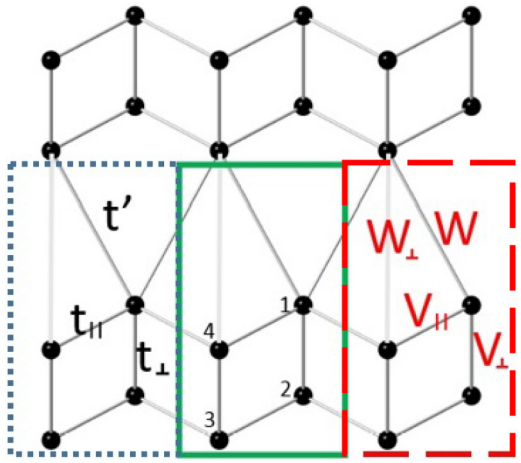

FIG. 1. (Color online) Schematic crystal structure of $Li_{0.9}Mo_6O_{17}$ projected onto the b-c plane showing only the partially filled Mo atoms forming the zigzag ladders relevant to the low-energy electronic properties. Our choice of unit cell is highlighted and the orbitals numerated (solid line) according to the text; the hoppings (dotted line) and the Coulomb interactions (dashed line) are also represented.

confirms the quasi-one-dimensionality of the Fermi surface. A Slater-Koster tight-binding parametrization of the system was proposed in Ref. [24] and the role of long-range Coulomb couplings in the anomalies of the metallic phase was also studied [27]. Here, we consider a strongly correlated model, which can capture the essential physics of $Li_{0.9}Mo_6O_{17}$ [24] consisting on an extended Hubbard lattice with four Mo atoms per unit cell, which reads

$$H = H_0 + H_U, \tag{1}$$

where H_0 is the noninteracting tight-binding Hamiltonian. The one-electron Hamiltonian can be expressed in terms of Bloch waves with the following nonzero matrix elements, the intraladder: $t_{12}(\mathbf{k}) = t_{43}(\mathbf{k}) = t_\perp = -0.024$ eV, and $t_{14} = t_{23}(\mathbf{k})t = 0.5$ eV and the hoppings among chains, $t_{13}(\mathbf{k}) = t' = 0.036$ eV, as is shown in Fig. 1 (dotted cell).

The diagonalized Hamiltonian, $H_0 = \sum_{\mathbf{k}\mu\sigma} \epsilon_\mu(\mathbf{k}) d^\dagger_{\mathbf{k}\mu\sigma} d_{\mathbf{k}\mu\sigma}$, leads to four bands denoted by μ; the two lowest ones cross the E_F [24,27,31]. The Fermi surface, close to one-quarter filling, $n = 0.225$, is shown in Fig. 2(a). Notice that the model includes four bands, two of them empty at energies three times higher than the Fermi level (0.75 eV), while we do not include two filled bands 0.2 eV below the Fermi energy [31].

The Coulomb interaction terms in the Hamiltonian includes on-site Hubbard interaction (U), intraladder interaction with the nonzero matrix elements $V_{12} = V_{32} = V_\parallel$ and $V_{12} = V_{34} = V_\perp$ and the interladder W interactions, $W_{13} = W$ and $W_{12} = W_{34} = W_\perp$, as shown in Fig. 1 (dashed cell):

$$H_U = U \sum_{l,i,\alpha} n^{(l)}_{i\alpha\uparrow} n^{(l)}_{i\alpha\downarrow} + \sum_{l,i,\alpha,j,\beta} V_{i\alpha,j\beta} n^{(l)\dagger}_{i\alpha} n^{(l)}_{j\beta} + \sum_{l,i,\alpha,j,\beta} W_{i\alpha,j\beta} n^{(l)}_{i\alpha} n^{(l+1)}_{j\beta}. \tag{2}$$

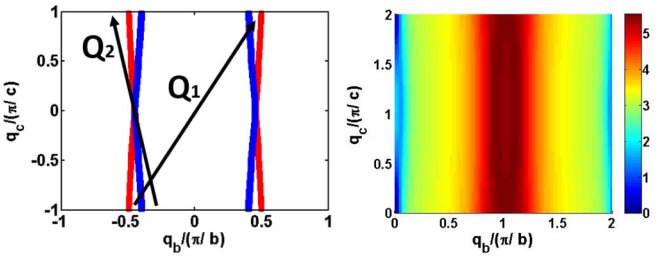

FIG. 2. (Color online) (a) Fermi surface with two bands, $\mathbf{Q_1}$ a nesting vector, and $\mathbf{Q_2}$ referred to in the text. (b) Real part of the bare susceptibility in momentum space for $\omega = 0$ and $q_a = 0$. Notice the maximum reveals the warping of the Fermi surface at the nesting vector.

The interacting Hamiltonian only includes density-density Coulomb interaction contributions. Within this work, we have considered several combinations of parameters, all of them leading to essentially the same results presented here where we reduce the parameter space to two variables (U and V). We take the Coulomb interaction among different sites with $1/|\mathbf{r}|$ dependence, where $|\mathbf{r}|$ is the distance among orbitals. Therefore, we parametrize the interactions by weighting the V's with the interatomic distances: $V = V_\parallel r_\parallel = V_\perp r_\perp = W r_W = W_\perp r_{W\perp}$. And $r_\parallel = 3.727$ Å, $r_\perp = 3.718$ Å, $r_W = 5.767$ Å, and $r_{W\perp} = 6.865$ Å.

III. MULTIORBITAL RPA APPROACH

In this section we explain the multiorbital RPA approach for this model; we study spin and charge ordering based on spin and charge susceptibility, respectively, and the superconducting vertex based on projections of different order parameters.

A. Spin susceptibility

The RPA spin susceptibility reads [32]

$$(\chi_s)_{\alpha,\beta}(\mathbf{q}) = (\chi_0)_{\alpha,\beta}(\mathbf{q}) + \sum_{\alpha'\beta'} (\chi_s)_{\alpha'\beta'}(\mathbf{q}) (U_s)^{\alpha'\beta'} (\chi_0)_{\alpha\beta}(\mathbf{q}), \tag{3}$$

where the indices α,β refer to the four Mo d_{xy} orbitals present in the unit cell. This is the more general case for density-density interactions. In our case the spin interaction is a diagonal matrix $(U_s)_{\alpha\beta} = U\delta_{\alpha,\beta}$ and momentum independent. The noninteracting susceptibility, χ_0, reads

$$(\chi_0)_{\alpha,\beta}(\mathbf{q}, i\omega) = -\frac{1}{N} \sum_{\mathbf{k},\mu,\nu} \frac{a^\alpha_\mu(\mathbf{k}) a^{\beta *}_\mu(\mathbf{k}) a^\beta_\nu(\mathbf{k}+\mathbf{q}) a^{\alpha *}_\nu(\mathbf{k}+\mathbf{q})}{i\omega + \epsilon_\nu(\mathbf{k}+\mathbf{q}) - \epsilon_\mu(\mathbf{k})} \times [f(\epsilon_\nu(\mathbf{k}+\mathbf{q})) - f(\epsilon_\mu(\mathbf{k}))], \tag{4}$$

where N is the number of lattice sites, and ν,μ are band indices. The matrix elements $a^\alpha_\mu(\mathbf{k}) = \langle \alpha | \mu \mathbf{k} \rangle$ are the coefficients of the eigenvectors diagonalizing H_0.

B. Charge susceptibility

The RPA charge susceptibility reads [32]

$$(\chi_c)_{\alpha,\beta}(\mathbf{q}) = (\chi_0)_{\alpha,\beta}(\mathbf{q}) - \sum_{\alpha'\beta'}(\chi_c)_{\alpha'\beta'}(\mathbf{q})(U_c)^{\alpha'\beta'}(\mathbf{q})(\chi_0)_{\alpha\beta}(\mathbf{q}), \tag{5}$$

where $U_c(\mathbf{q})$ is the Coulomb matrix appearing in Eq. (2) expressed in momentum space, $(U_c)_{\alpha\beta}(\mathbf{q}) = U\delta_{\alpha,\beta} + 2\hat{V}(\mathbf{q})_{\alpha,\beta}$, where $\hat{V}(\mathbf{q})$ is the Fourier transform of $V_{i\alpha,j\beta}$ and $W_{i\alpha,j\beta}$ interactions in real space.

C. Superconducting vertex

Assuming that the pairing interaction arises from the exchange of spin and charge fluctuations, we can calculate the pairing vertex using the RPA. (For a detailed description of the method, see, for instance, Ref. [32].) The strength of the interaction is weighted by ω^{-1} and by making use of the Kramers-Kronig relation we only need the real zero-frequency vertex [32]. For the multiorbital case [33,34], singlet and triplet pairing vertices at zero frequency are given by

$$\Gamma^{\text{singlet}}_{\alpha\beta}(\mathbf{k},\mathbf{k}') = \big(U + \tfrac{3}{2}U_s\chi_s(\mathbf{k}-\mathbf{k}')U_s + \hat{V}(\mathbf{k}-\mathbf{k}') - \tfrac{1}{2}U_c(\mathbf{k}-\mathbf{k}')\chi_c(\mathbf{k}-\mathbf{k}')U_c(\mathbf{k}-\mathbf{k}')\big)_{\alpha\beta}, \tag{6}$$

$$\Gamma^{\text{triplet}}_{\alpha\beta}(\mathbf{k},\mathbf{k}') = \big(-\tfrac{1}{2}U_s\chi_s(\mathbf{k}-\mathbf{k}')U_s + \hat{V}(\mathbf{k}-\mathbf{k}') - \tfrac{1}{2}U_c(\mathbf{k}-\mathbf{k}')\chi_c(\mathbf{k}-\mathbf{k}')U_c(\mathbf{k}-\mathbf{k}')\big)_{\alpha\beta}. \tag{7}$$

We transform the vertex in real space $\alpha\beta$ into momentum space $\mu\nu$ with the band-structure eigenvalues $a^{\alpha}_{\mu}(\mathbf{k})$. The Cooper pairs have an incoming momentum of $(\mathbf{k},-\mathbf{k})$ and an outgoing momentum of $(\mathbf{k}',-\mathbf{k}')$. We take the symmetric and antisymmetric parts for singlet and triplet channels, respectively:

$$\Gamma^{\text{singlet}}_{\mu\nu}(\mathbf{k},\mathbf{k}') = \sum_{\alpha\beta} a^{\alpha*}_{\mu}(-\mathbf{k})a^{\alpha*}_{\mu}(\mathbf{k})\text{Re}\big[\Gamma^{\text{singlet}}_{\alpha\beta}(\mathbf{k},\mathbf{k}')\big] \times a^{\beta}_{\nu}(\mathbf{k}')a^{\beta}_{\nu}(-\mathbf{k}') + (\mathbf{k}' \leftrightarrow -\mathbf{k}'), \tag{8}$$

$$\Gamma^{\text{triplet}}_{\mu\nu}(\mathbf{k},\mathbf{k}') = \sum_{\alpha\beta} a^{\alpha*}_{\mu}(-\mathbf{k})a^{\alpha*}_{\mu}(\mathbf{k})\text{Real}\big[\Gamma^{\text{triplet}}_{\alpha\beta}(\mathbf{k},\mathbf{k}')\big] \times a^{\beta}_{\nu}(\mathbf{k}')a^{\beta}_{\nu}(-\mathbf{k}') - (\mathbf{k}' \leftrightarrow -\mathbf{k}'). \tag{9}$$

We solve the gap equation by projecting out s, p, d, and f waves [35]:

$$\lambda_\gamma = -\frac{\sum_{\mu\nu}\int_{FS}\frac{d^2\mathbf{k}'_\mu}{|v_F(\mathbf{k}'_\mu)|}\int_{FS}\frac{d^2\mathbf{k}_\nu}{|v_F(\mathbf{k}_\nu)|}g_\gamma(\mathbf{k}'_\mu)\Gamma^{\text{P}}_{\mu\nu}(\mathbf{k},\mathbf{k}')g_\gamma(\mathbf{k}_\nu)}{\sum_{\mu}\int_{FS}\frac{d^2\mathbf{k}_\mu}{|v_F(\mathbf{k}_\mu)|}g^2_\gamma(\mathbf{k}_\mu)} \tag{10}$$

where γ numerates the different waves projected (s, p, d, or f) and P depends on the γ symmetry. P could be singlet or triplet. The gap equation has a solution when λ_γ is 1. We increase the interaction parameters until the dominant wave solves the equation; for stronger interactions the gap is already opened in that channel.

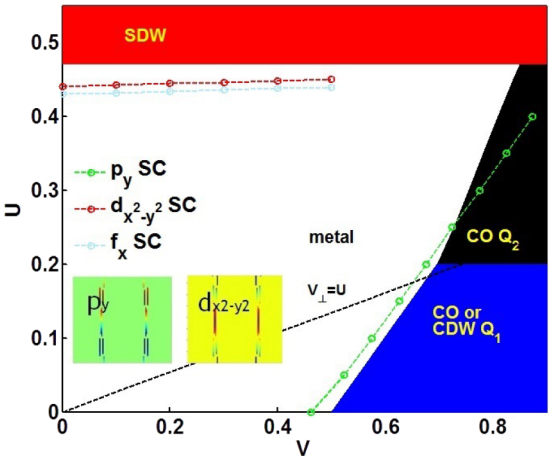

FIG. 3. (Color online) (a) Phase diagram U-V. Extended region of p_y superconductivity with nodes in the Fermi surface (inset) close to the CO region. In the inset we show $d_{x^2-y^2}$ and p_y wave functions.

IV. PHASE DIAGRAM

Using the parametrization described in Sec. II we can study the complete parameter space, reduced to two variables U and V. The RPA spin susceptibility [Eq. (3)] breaks at $U = 0.47$ indicating a spin-density wave (SDW) phase.

The RPA charge susceptibility [Eq. (5)] diverges for different momenta for different U on-site Hubbard interaction, leading to different charge-order regions in the phase diagram (see Fig. 3). The charge-order susceptibility divergence consists in an interplay between the bare susceptibility strongly peaked at $q_b \approx \pi$ [Fig. 2(b)] and the charge interaction $U_c(\mathbf{q})$. The analysis involves 4×4 terms but in essence can be understood with the sum of the 16 contributions. We observe that $U_c(\mathbf{q})$ [Fig. 4(c)] is a minimum at the $(2\pi,2\pi)$ edge of the Brillouin zone. Notice that the periodicity is not required since we are dealing with the sum of the elements of a matrix. For $U = 0$, red means positive and blue negative; for that reason, among all nesting vectors ($q_b \approx \pi$), $\mathbf{Q_1}$ diverges first. The divergence at this momentum stems from nesting.

As long as we increase U, $U_c(\mathbf{q})$ remains negative in a smaller region, leading to the displacement of the divergence to $\mathbf{Q_2}$. The reason why $\mathbf{Q_2}$ does not change with U can be understood from the bare susceptibility structure, χ_0. χ_0 in the entire Brillouin zone (only q_b matters, Fig. 2) can be divided

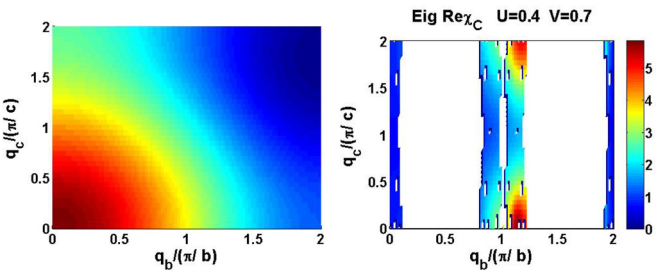

FIG. 4. (Color online) Left: Momentum space distribution of the interaction, showing the sum of all components. Right: The same as in Fig. 5 (bottom right), in those momenta relevant to the pairing vertex.

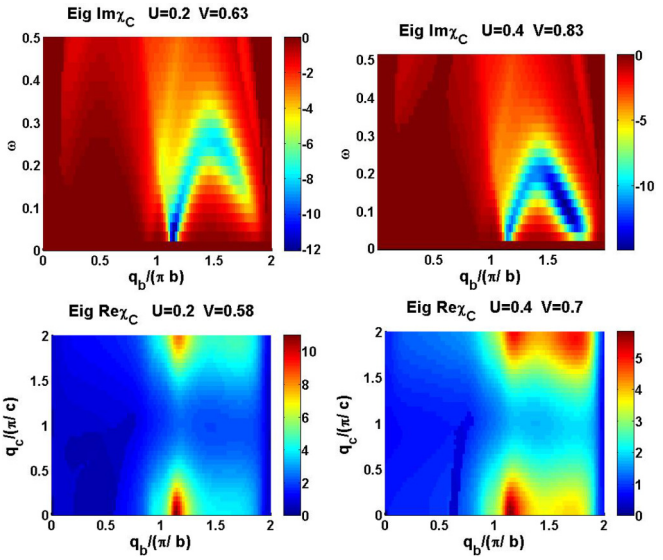

FIG. 5. (Color online) Top: Imaginary part of the larger eigenvalue of the charge susceptibility near the critical value (see Fig. 3) for (left) $U = 0.2$ and (right) $U = 0.4$. Bottom: Real part of the larger eigenvalue in momentum space and zero frequency close to the critical value for (left) $U = 0.2$ and (right) $U = 0.4$.

into three zones: $0 < q_b \lesssim 0.1\pi/b$, $0.1\pi/b \lesssim q_b \lesssim 0.6\pi/b$, and $0.6\pi/b \lesssim q_b < \pi/b$ (and symmetric regions with respect to $q_b = pi/b$). In the first zone the susceptibility increases sharply due to the warping. By increasing q_b we can connect more points of the Fermi surface. In the second region the system only has access to the Fermi sheets at one side, increasing weakly the value of the particle-hole susceptibility. In the third region connections among the two pairs of sheets gives also a strong enhancement with momentum. In our case, the range of U below the SDW ordered phase makes the negative $U_c(\mathbf{q})$ to be in the second region of the bare susceptibility. Since this region of χ_0 is weakly q dependent, we observe a minimal change of $\mathbf{Q_2}$ with increasing U. The divergence of the charge susceptibility at this momentum is due to interactions, and the softening can be described as a critical mode similar to the one found in Ref. [27]. In Fig. 6 we see a critical exponent of $\frac{1}{2}$.

The transition from $\mathbf{Q_1}$ to $\mathbf{Q_2}$ ordering phases is also shown in Fig. 5. The upper panels show the frequency against momentum of the charge susceptibility (maximum eigenvalue, which is significantly larger than the other three). Notice that above $\omega > 0.2$ contributions from completely filled bands, ignored by the model, are expected. The lower panels show the charge susceptibility (maximum eigenvalue) at zero frequency. On the left-hand hand panels $U = 0.2$ while on the right-hand panels $U = 0.4$. We observe a change in the spectral weight of the collective mode from $\mathbf{Q_1}$ to $\mathbf{Q_2}$ when U is increased. Moreover, while the weight at $\mathbf{Q_1}$ exists at any value of V, at $\mathbf{Q_2}$ the mode softens, signaling at the proximity to the transition.

Near the SDW region we found superconductivity in $d_{x^2-y^2}$ channel. This behavior is consistent with that expected for a quasi-one-dimensional square lattice at quarter filling [36]. A very recent preprint [28] proposes an order parameter with different sign in each band and a total of three node planes in

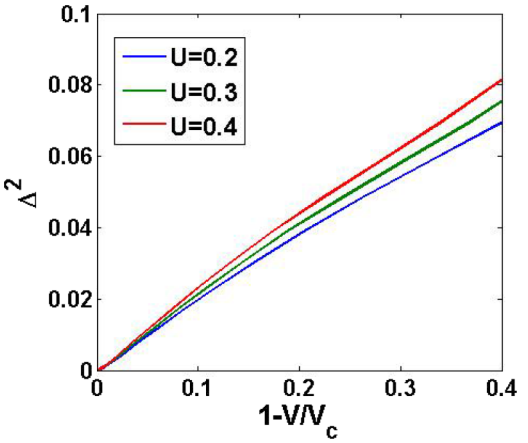

FIG. 6. (Color online) Gap squared of the $\mathbf{Q_2}$ critical mode scaled with the critical interaction $V = V_c$. We observe a $\frac{1}{2}$ exponent near the critical value.

the b direction (and two more in the c direction) at $V = 0$. We skip the bracketed description and project the wave (here we call it f_x) with our methodology. The results (Fig. 3) show that both d and f channels are very close, with the f_x dominating.

As long as experiments do not show signatures of SDW gap opening or magnetic response [37], we can work with lower U values to avoid strong spin fluctuations. The Coulomb interactions are comparable with Ref. [26].

Near the CDW or CO regions of the phase diagram we found triplet superconductivity in the p_y channel, with nodes at the Fermi surface. Near the $\mathbf{Q_1}$ CDW region, we found a narrow stripe [38] of superconductivity due to charge fluctuations at $\mathbf{Q_1}$. We observe that $\mathbf{Q_1}$ is a nesting vector connecting all the Fermi surface with different phases of the order parameter. See the inset in Fig. 3. We have included a dashed line indicating where the extended Hubbard interaction $V_\perp$ equals U. The parameters are meaningful above this line, but since this is an effective model, we can expect the study to be physical even slightly below the $V_\perp = U$ line.

From this study, apparently we can design the interactions in Fig. 4(c) to be a minimum in a given momentum, in such a way that favors superconductivity with a certain order parameter. Nevertheless, we need to take into account the bare susceptibility structure and the orbital distribution in real space. In the present model, the bare susceptibility is peaked at $q_b \approx \pi$, and the divergence at $\mathbf{Q_1}$ is favored by perpendicular Coulomb interactions $V_\perp$ and $W_\perp$, whereas interactions along the chains do not distinguish momenta in the b direction.

The $\mathbf{Q_2}$ momentum is not involved in the vertex calculation [Eq. (10)], so we are still able to work with the superconducting vertex since it has not diverged. In that region, strong charge fluctuations still persist at $\mathbf{Q_1}$ due to nesting, and superconductivity would be found if another charge-ordered phase were not present.

Coexistence in the model

If the order parameter of the CO is small, and assuming that the $\mathbf{Q_2}$ modulation does not open a gap at E_F, we consider now the possibility of coexistence with superconductivity (SC) in this model, even though it may not have relevance for the material.

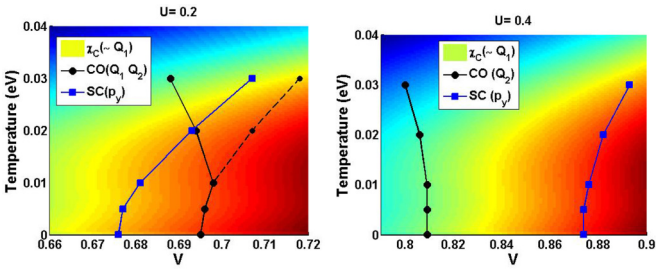

FIG. 7. (Color online) The background represents the charge fluctuations near $\mathbf{Q_1}$ and on top of that are the CO transition line (green) and superconducting transition line (solid black) for (left) $U = 0.2$ and (right) $U = 0.4$. The dashed black line is the CO transition due to $\mathbf{Q_1}$ if the other order is not present. The blue line is the superconducting transition.

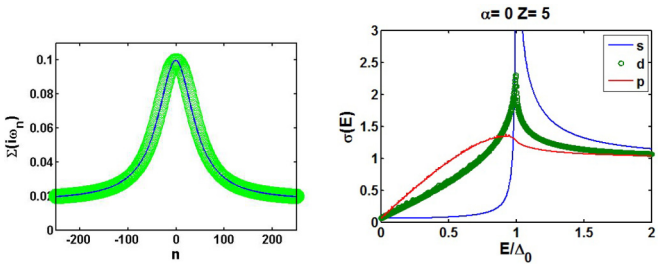

FIG. 8. (Color online) Left: Gap in the Matsubara frequency ($i\omega_n$) at $T = 0.01$, $U = 0.2$, and $V = 0.676$, green line; Lorentzian fit, blue line. Right: Conductance against energy for different superconducting order parameters. We can distinguish the p_y wave; α is the angle of the order parameter with the junction, and Z is the height of the tunnel barrier, in this case the insulating phase [40].

We study the coexisting region with temperature (see Fig. 7). The charge fluctuations have a reentrant behavior in the RPA approach [39], due to the fact that the bare susceptibility $\chi_0(\mathbf{q},\omega)$ is maximum in energy ($\omega \ll t$) when $\mathbf{q}$ connects different points of the band structure approximately ω away from Fermi level. In that case $\mathbf{Q_1}$ is a nesting vector and the maximum is close in energy, $\omega = 0.01 \approx T$. However, $\mathbf{Q_2}$ exhibits its peak of reentrant behavior at a larger energy, and we only see the decrease of critical V with temperature. In Fig. 7(a) the critical momentum changes from Q_1 at low temperatures to Q_2. We observed that change from charge susceptibility and it is represented by the change of behavior of the CO line. The temperature makes the bare susceptibility softer, lowering the value of $\chi_0(\mathbf{Q_1})$ and shifting the critical momentum to Q_2.

V. ELIASHBERG EQUATION WITH A REDUCED VERTEX

In the previous section we showed that the superconducting vertex is dominated by the charge susceptibility near $\mathbf{Q_1}$ [see Eq. (10)]. The result is that by using just a few vertex momenta we reproduce the λ_{py} value. However, we cannot reduce easily the four-orbital model for a simpler tight binding, since near $\mathbf{Q_1}$ the bands have a similar weight in the four orbitals. For that reason, we select the larger values of the pairing vertex [calculated with the four-orbital model, Eqs. (8) and (9)] and as a result, we see that less than 10% of the vertex is enough to get more than 90% of the λ_{py} value. In order to reproduce λ_{py} from momenta near $\mathbf{Q_1}$ we need to multiply the value of the vertex by 4; otherwise we need to include momenta near $\mathbf{q} = 0$ because it is significantly large and connects many pairs of Fermi surface momenta.

Moreover, we see that the value of the pairing vertex is almost independent of q_y. All those simplifications allow us to work with a simpler model and solve the linear Eliashberg equation in Matsubara frequencies, given by

$$\lambda_{py}\Sigma(\mathbf{k},i\omega_n) = \frac{-1}{N}\sum_{\mathbf{k}'i\omega_n'} G^0(\mathbf{k}',i\omega_n')\Gamma^{\text{triplet}}(\mathbf{k},\mathbf{k}',i\omega_n - i\omega_n') \times G^0(-\mathbf{k}',-i\omega_n')\Sigma(\mathbf{k}',i\omega_n'), \quad (11)$$

where

$$G^0(\mathbf{k}',i\omega_n')_{sp} = \sum_\nu \frac{a_\nu^s(\mathbf{k})a_\nu^p(\mathbf{k})}{i\omega_n - \epsilon_\nu(\mathbf{k})} \quad (12)$$

are 4×4 matrices, and Γ^{triplet} is also a matrix defined in Eq. (9) but with $i\omega_n$ dependence coming from the bare susceptibility [Eq. (4) in Eq. (7)]. We calculate the momentum dependence of the gap by projecting on the p_y order parameter: $\Sigma(\mathbf{k},i\omega_n) = f(i\omega_n)\sin(k_c c)$. The result (shown in Fig. 8) can be fitted by a Lorentzian plus a constant; analytic continuation or Padé approximants gives the same result: a real constant for the relevant frequencies. Provided the gap value is small, only low frequencies are relevant for experiments, as normal-insulator superconducting junctions [40] [see Fig. 8(b)].

VI. DISCUSSION AND CONCLUSIONS

As was previously mentioned, $Li_{0.9}Mo_6O_{17}$ exhibits signatures of Luttinger liquid behavior for a wide range of temperatures. Thus, it is important to discuss its relation with the physics described above.

In Fig. 9, we present a schematic phase diagram for the model and consider its relevance for the physics of LiPB. Merging the renormalization-group estimation of the crossover temperature and the RPA calculations for the CDW, and

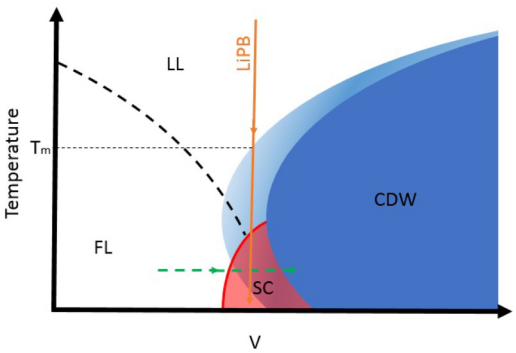

FIG. 9. (Color online) Schematic phase diagram for LiPB. The present study comprises the green horizontal arrow; we believe the temperature dependence of the real material is represented by the vertical orange arrow.

considering the fluctuation exchange in the superconducting vertex, we compose a schematic diagram (Fig. 9). At high temperatures, the metallic phase is a LL. As the temperature goes down, the perpendicular hopping drives the system through a crossover to a Fermi liquid and the interchain Coulomb interactions through a thermodynamic phase transition to a CDW. Our analysis of the SC vertex comprises the dashed horizontal line. Since we are working at temperatures well below T_{LL}, the use of RPA, as a perturbation theory of the essentially free electron system, is well justified as a starting point. In other words, we are able to describe the superconductivity as an instability of a Fermi liquid, in spite of the normal phase of the material being a LL. On the other hand, the behavior of the material as the temperature goes down seems to be represented by the solid vertical line. This statement is based on the spectroscopies [9,10] at temperatures right above T_c. The density of states show power-law behavior very similar to that observed at much higher temperatures and similar values of α. Placing the material slightly on the left of that vertical line would imply an interesting crossover from one non-Fermi liquid (NFL) (the LL) to another NFL (FL + strong charge fluctuations). At a purely qualitative level, no evidence of a Fermi edge developing at low temperatures has been observed and the experimental values of α seem to increase (instead of decrease). However, both alternatives rely on details of the model and should be quantitatively contrasted with the spectroscopies.

The dashed line in Fig. 9 shows the dimensional crossover from Luttinger liquid to Fermi liquid [41,42]. The small value of the perpendicular hopping suggests considering it as a perturbation. Based on the renormalization-group approach, we can estimate the crossover temperature to be $T_{LL} \sim t(\frac{t_\perp}{t})^{\frac{1}{1-\alpha}}$, where α is the exponent for the single-particle density of states. In Fig. 10 we show the estimated dimensional crossover for Luttinger chains coupled with Hubbard and V interactions. The value of α is computed using interaction parameters U and V following the CO border shown in Fig. 3. W is set to zero. Note that the same Coulomb interactions driving the charge ordering allow for large values of α. Therefore, we expect T_{LL} to be very small when the CDW is approached. This fact opens the possibility for a direct transition from the LL to the superconducting phase. It would be interesting to study this possibility with techniques similar to those used in Ref. [43].

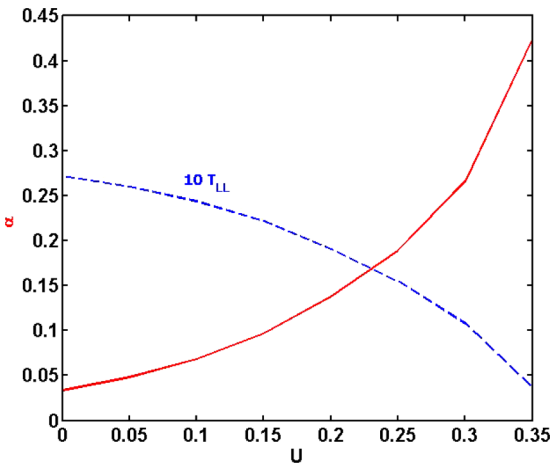

FIG. 10. (Color online) Dashed line, renormalization group estimation of the crossover temperature for the critical V values found for each U; solid line, the exponent in the Luttinger density of states, α.

The charge-ordering transition for the RPA apparently occurs at arbitrarily large temperatures as V increases, but we expect the slight modifications presented in Ref. [44], which considers how the fluctuation effects modify the Green's function self-consistently, evaluating also vertex corrections. Other details like the reentrant behavior for the charge-ordering transition, typical of RPA calculations, are unessential for the physics of the system.

Since our results imply a nodal wave function, a discussion of the experimentally measured specific heat jump is necessary. From a strict BCS approach, the value of the normalized specific heat jump should be smaller than the BCS result, $\Delta C/\gamma T_c = 1.43$. However, in strong coupling or when the pairing mechanism is due to either spin or charge fluctuations the argument may be different. From a detailed study on the spin-fluctuation effect, Williams *et al.* [45] observed that both ratios $T_c/\Delta(0)$ and $\Delta C/\gamma T_c$ are not universal numbers but depend strongly on the functional form of the pairing-fluctuation spectrum. Actually, the influence of the low-frequency fluctuations increases the jump and overcomes the effect of the nodes in the order parameter. Based on this study, we can argue that a nodal order parameter can give rise to a normalized specific heat jump of 2.07 as measured [16]. This study requires a comment on the filled bands close to the Fermi level and not taken into account in the model.

Due to the use of the Kramers-Kronig relation, the real part of the vertex at zero frequency [Eqs. (8) and (9)] includes information about the model band structure at any frequency weighted by ω^{-1} through the function $\mathrm{Im}(\chi_c(Q1,\omega)/\omega)$. We expect the charge divergence to dominate at $\mathbf{Q_1}$ even in the presence of those bands, because $\mathbf{Q_1}$ is a nesting vector. The top of the bands are 0.2 eV away from Fermi level [31] (a slightly larger difference according to experiments [7]), but the RPA particle-hole excitation constructed with a particle of these filled bands at $\mathbf{Q_1}$ requires a hole in another band; an energy of at least 0.3 eV is needed (estimation made from DFT band structure [31]). The validity of the model concerning superconductivity and charge order is guaranteed

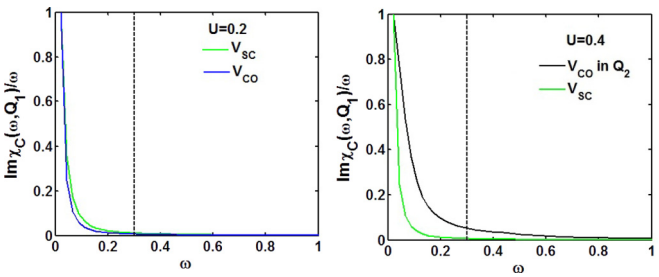

FIG. 11. (Color online) Normalized imaginary part of the charge susceptibility at $\mathbf{Q_1}$ weighted by ω^{-1} against frequency for different interaction parameters. $U = 0.2$ (left) and $U = 0.4$ (right) and V at the superconducting transition and CDW or CO transition. Dashed lines show the energy at which bands not taken into account in the model would contribute at such internal momentum.

since the energy of relevant phenomena is considerably below the influence of nonconsidered bands, as we can observe in Fig. 11. We expect a contribution to the vertex at energy $\omega \approx 0.3$ eV (dashed line in Fig. 11), which is considerably away from the relevant energy scale of the physics described here.

To summarize, we have studied a microscopic extended Hubbard model for LiPB. We have characterized the couplings promoting SC close to different charge- ordering patterns. A detailed analysis within the RPA of the vertex shows triplet superconductivity with nodes on the Fermi surface close to those ordered phases. The relevance of these results is discussed in terms of the general experimental perspective of the material.

ACKNOWLEDGMENTS

We thank J. W. Allen, J. Merino, H. Suderow, and L. Taillefer for fruitful discussions. We acknowledge financial support from MINECO Grant No. FIS2012-37549-C05-03.

[1] J. D. Denlinger, G. H. Gweon, J. W. Allen, C. G. Olson, J. Marcus, C. Schlenker, and L. S. Hsu, Phys. Rev. Lett. **82**, 2540 (1999).
[2] G.-H. Gweon *et al.*, J. Electron Spectrosc. Relat. Phenom. **117-118**, 481 (2001).
[3] G.-H. Gweon *et al.*, Physica B **312-313**, 584 (2002).
[4] J. W. Allen, Solid State Commun. **123**, 469 (2002).
[5] G.-H. Gweon, J. W. Allen, and J. D. Denlinger, Phys. Rev. B **68**, 195117 (2003).
[6] G.-H. Gweon, S. K. Mo, J. W. Allen, J. He, R. Jin, D. Mandrus, and H. Hochst, Phys. Rev. B **70**, 153103 (2004).
[7] F. Wang, J. V. Alvarez, S.-K. Mo, J. W. Allen, G.-H. Gweon, J. He, R. Jin, D. Mandrus, and H. Hochst, Phys. Rev. Lett. **96**, 196403 (2006).
[8] F. Wang, J. V. Alvarez, J. W. Allen, S.-K. Mo, J. He, R. Jin, D. Mandrus, and H. Hochst, Phys. Rev. Lett. **103**, 136401 (2009).
[9] L. Dudy, J. D. Denlinger, J. W. Allen, F. Wang, J. He, D. Hitchcock, A. Sekiyama, and S. Suga, J. Phys.: Condens. Mattter **25**, 014007 (2013).
[10] J. Hager, R. Matzdorf, J. He, R. Jin, D. Mandrus, M. A. Cazalilla, and E. W. Plummer, Phys. Rev. Lett. **95**, 186402 (2005).
[11] T. Podlich, M. Klinke, B. Nansseu, M. Waelsch, R. Bienert, J. He, R. Jin, D. Mandrus, and R. Matzdorf, J. Phys.: Condens. Matter **25**, 014008 (2013).
[12] N. Wakehman, A. F. Bangura, X. Xu, J.-F. Mercure, M. Greenblatt, and N. E. Hussey, Nat. Commun. **2**, 396 (2011).
[13] M. Greenblatt, W. H. McCarroll, R. Neifeld, M. Croft, and. J. V. Waszczak, Solid State Commun. **51**, 671 (1984).
[14] C. Escribe-Filippini, J. Beille, M. Boujida, J. Marcus, and C. Schlenker, Physica C **162-164**, 427 (1989).
[15] J. Choi, J. L. Musfeldt, J. He, R. Jin, J. R. Thompson, D. Mandrus, X. N. Lin, V. A. Bondarenko, and J. W. Brill, Phys. Rev. B **69**, 085120 (2004).
[16] J.-F. Mercure, A. F. Bangura, Xiaofeng Xu, N. Wakeham, A. Carrington, P. Walmsley, M. Greenblatt, and N. E. Hussey, Phys. Rev. Lett. **108**, 187003 (2012).
[17] C. Schlenker, J. Dumas, C. Escribe-filippini, H. Guyot, J. Marcus, and G. Fourcaudot, Philos. Mag. B **52**, 643 (1985).
[18] S. van Smaalen, Acta Crystallogr. A **61**, 51 (2005).
[19] C. A. M. dos Santos, B. D. White, Y. K. Yu, J. J. Neumeier, and J. A. Souza, Phys. Rev. Lett. **98**, 266405 (2007).
[20] M. S. da Luz, J. J. Neumeier, C. A. M. dos Santos, B. D. White, H. J. I. Filho, J. B. Leao, and Q. Huang, Phys. Rev. B **84**, 014108 (2011).
[21] J. L. Cohn, S. Moshfeghyeganeh, C. A. M. dos Santos, and J. J. Neumeier, Phys. Rev. Lett. **112**, 186602 (2014).
[22] G. Wu, B. Wu, and W. G. Clark, arXiv:1410.7793.
[23] A. G. Lebed and O. Sepper, Phys. Rev. B **87**, 100511(R) (2013); O. Sepper and A. G. Lebed, *ibid.* **88**, 094520 (2013).
[24] J. Merino and R. H. McKenzie, Phys. Rev. B **85**, 235128 (2012).
[25] P. Chudzinski, T. Jarlborg, and T. Giamarchi, Phys. Rev. B **86**, 075147 (2012); T. Jarlborg, P. Chudzinski, and T. Giamarchi, *ibid.* **85**, 235108 (2012).
[26] M. Nuss and M. Aichhorn, Phys. Rev. B **89**, 045125 (2014).
[27] J. Merino and J. V. Alvarez, Phys. Rev. B **91**, 035135 (2015).
[28] W. Cho, C. Platt, Ross H. McKenzie, and S. Raghu, Phys. Rev. B **92**, 134514 (2015).
[29] M. Onoda, K. Toriumi, Y. Matsuda, and M. Sato, J. Solid State Chem. **66**, 163 (1987).
[30] M.-H. Wangbo and E. Canadell, J. Am. Chem. Soc. **110**, 358 (1988).
[31] Z. S. Popović and S. Satpathy, Phys. Rev. B **74**, 045117 (2006).
[32] S. Graser, T. A. Maier, P. J. Hirschfeld, and D. J. Scalapino, New J. Phys. **11**, 025016 (2009).
[33] T. Takimoto, T. Hotta, and K. Ueda, Phys. Rev. B **69**, 104504 (2004).
[34] S. Onari, R. Arita, K. Kuroki, and H. Aoki, Phys. Rev. B **70**, 094523 (2004).
[35] D. J. Scalapino, E. Loh, and J. E. Hirsch, Phys. Rev. B **34**, 8190 (1986).
[36] H. Shimahara, J. Phys. Soc. Jpn. **58**, 1735 (1989); K. Kuroki and H. Aoki, Phys. Rev. B **60**, 3060 (1999); H. Kino and H. Kontani, J. Low. Temp. Phys. **117**, 317 (1999).
[37] Y. Matsuda, M. Sato, M. Onoda, and K. Nakao, J. Phys. C **19**, 6039 (1986).
[38] We find that in order to generate pairing eigenvalues of order 1, we need to work within the RPA at interaction strengths quite close to the charge (or spin) instability. However, Graser *et al.* [32] mention that, from the earlier experience comparing RPA with quantum Monte Carlo results on the single-band Hubbard model [46], one should expect that the bare interaction parameters appearing in the RPA expressions are renormalized, such that one is actually not so close to the true instability.
[39] J. Merino, A. Greco, N. Drichko, and M. Dressel, Phys. Rev. Lett. **96**, 216402 (2006).
[40] Y. Tanaka and S. Kashiwaya, Phys. Rev. Lett. **74**, 3451 (1995).

[41] T. Giamarchi, Chem. Rev. **104**, 5037 (2004).
[42] D. Boies, C. Bourbonnais, and A.-M. S. Tremblay, Phys. Rev. Lett. **74**, 968 (1995).
[43] J. V. Alvarez and J. Gonzalez, Phys. Rev. Lett. **91**, 076401 (2003); J. Gonzalez and J. V. Alvarez, Phys. Rev. B **70**, 045410 (2004).
[44] K. Yoshimi, T. Kato, and H. Maebashi, J. Phys. Soc. Jpn. **78**, 104002 (2009).
[45] P. J. Williams and J. P. Carbotte, Phys. Rev. B **39**, 2180 (1989).
[46] T. A. Maier, A. Macridin, M. Jarrell, and D. J. Scalapino, Phys. Rev. B **76**, 144516 (2007).